Kinetic Mechanism of Adenine Phosphoribosyltransferase from *Leishmania donovani*†

Caleb Bashor, John M. Denu, Richard G. Brennan, and Buddy Ullman*

Department of Biochemistry and Molecular Biology, Oregon Health & Science University, 3181 SW Sam Jackson Park Road, Portland, Oregon 97201-3098

Received October 19, 2001; Revised Manuscript Received January 14, 2002

ABSTRACT: Adenine phosphoribosyltransferase (APRT, EC 2.4.2.7) catalyzes the reversible phosphoribosylation of adenine from α-D-5-phosphoribosyl-1-pyrophosphate (PRPP) to form AMP and PP_i. Three-dimensional structures of the dimeric APRT enzyme from *Leishmania donovani* (LdAPRT) bear many similarities to other members of the type 1 phosphoribosyltransferase family but do not reveal the structural basis for catalysis (Phillips, C. L., Ullman, B., Brennan, R. G., and Hill, C. P. (1999) *EMBO J. 18*, 3533−3545). To address this issue, a steady state and transient kinetic analysis of the enzyme was performed in order to determine the catalytic mechanism. Initial velocity and product inhibition studies indicated that LdAPRT follows an ordered sequential mechanism in which PRPP is the first substrate to bind and AMP is the last product to leave. This mechanistic model was substantiated by equilibrium isotope exchange and fluorescence binding studies, which provided dissociation constants for the LdAPRT−PRPP and LdAPRT−AMP binary complexes. Pre-steady-state kinetic analysis of the forward reaction revealed a burst in product formation indicating that phosphoribosyl transfer proceeds rapidly relative to some rate-limiting product release event. Transient fluorescence competition experiments enabled measurement of rates of binary complex dissociation that implicated AMP release as rate-limiting for the forward reaction. Kinetics of product ternary complex formation were evaluated using the fluorophore formycin AMP and established rate constants for pyrophosphate binding to the LdAPRT−formycin AMP complex. Taken together, these data enabled the complete formulation of an ordered bi−bi kinetic mechanism for LdAPRT in which all of the rate constants were either measured or calculated.

Adenine phosphoribosyltransferase (APRT)[1] is a purine salvage enzyme that catalyzes the Mg^{2+}-dependent transfer of the 5-phosphoribosyl moiety from α-D-5-phosphoribose-1-pyrophosphate (PRPP) to adenine, resulting in the formation of AMP and inorganic pyrophosphate (PP_i). Although APRT is functionally redundant in mammals and most other organisms that can generate AMP de novo, via the purine biosynthetic pathway, recycling of preformed purines by purine salvage enzymes does play an important role in periods of rapid growth such as tumor proliferation and embryogenesis (*1*). Although APRT deficiency in humans is not lethal, it causes 2,8-dihydroxyadenine urinary lithiasis (a rare form of kidney stones). In contrast to the mammalian situation, protozoan parasites lack the ability to synthesize purine nucleotides de novo, and each genus has consequently evolved a unique complement of purine salvage enzymes that enable it to scavenge host purines (*2*). The indispensable nutritional function of the purine salvage pathway of protozoan parasites, therefore, offers a multiplicity of potential targets for therapeutic validation. APRT is an important component of the purine salvage pathway for many (but not all) protozoan parasites and is likely to be essential for several genera.

APRT is a member of the type I phosphoribosyltransferase (PRT) family, enzymes that play roles in both the de novo and salvage pathways of purines, pyrimidines, and pyridines, as well as in several amino acid biosynthetic pathways in lower organisms. The structures of many type I PRTs have now been solved, and each shares a common core region of at least five parallel strands surrounded by three or more helices (*3*). This core encompasses a conserved domain of 13 amino acid residues known as the PRPP binding motif that binds the ribose ring and 5′ phosphate of either PRPP or nucleotides in crystal structures of PRTs complexed with either substrate or product, respectively (*4*−*7*). Type I PRTs also possess a structurally versatile region known as the hood, which confers substrate selectivity to the enzyme, and a flexible loop that closes over the active site during catalysis (*4*−*7*).

On the basis of early steady-state kinetic and isotope exchange studies performed on type I PRTs, including orotate PRT (OPRT), uracil PRT (UPRT), and hypoxanthine-guanine PRT (HGPRT), a ping-pong (covalent intermediate) type mechanistic model was proposed for PRT catalysis (*8*−*10*).

† Supported by Grant RO-37 AI23682 to B.U. from the National Institutes of Health and Grant R0-1 GM59785 to J.M.D.

* To whom correspondence should be addressed. Tel: (503) 494-8437. Fax: (503) 494-8393. E-mail: ullmanb@ohsu.edu.

[1] Abbreviations: APRT, adenine phosphoribosyltransferase; PRPP, α-D-5-phosphoribose-1-pyrophosphate; PP_i, inorganic pyrophosphate; PRT, phosphoribosyltransferase; OPRT, orotate phosphoribosyltransferase; UPRT, uracil phosphoribosyltransferase; HGPRT, hypoxanthine-guanine phosphoribosyltransferase; LdAPRT, *Leishmania donovani* APRT; TNP-AMP, trinitrophenyl-AMP; QPRT, quinolinate phosphoribosyltransferase.

10.1021/bi0158730 CCC: $22.00
Published on Web 03/03/2002

In contrast, both Henderson et al. (*11*) and Giacomello and Salerno (*12*) proposed a sequential reaction mechanism for the human HGPRT on the basis of extensive steady-state kinetic analyses. More recent mechanistic studies with recombinant HGPRTs, employing both steady-state and pre-steady-state kinetics, have convincingly demonstrated that HGPRT proceeds through a fully ordered bi−bi sequential mechanism in which PRPP is the first substrate to bind to the enzyme followed by the purine base (*13*−*15*). Kinetics of recombinant OPRT from *Salmonella typhimurium* have also been studied recently by a variety of techniques, and the enzyme was shown to follow a random sequential mechanism (*16*, *17*). These latter kinetic studies on the *S. typhimurium* OPRT further demonstrated that early isotope exchange data (*8*) that were initially interpreted as evidence for a ping-pong type mechanism for OPRT were artifactual (*16*), further bolstering the consensus that type I PRTs all follow sequential mechanisms that proceed through reversible substrate ternary complex formation.

Compared to other purine and pyrimidine PRTs, investigations of APRT enzymes have been scant. Biochemical studies on APRT from rat liver (*18*, *19*), *Plasmodium falciparum* (*20*), and *Saccharomyces cerevisiae* (*22*) have demonstrated divalent cation dependence, pH optima, and kinetic constants similar to other purine PRTs. Ping-pong type kinetic mechanisms involving an activated phosphoribosyl intermediate have also been proposed for the human and yeast APRTs (*18*, *21*), but there has, as of yet, been no demonstration of an enzyme−phosphoribose covalent complex by isotope exchange for either of these enzymes. Relatively recently, three-dimensional structures of the *S. cerevisiae* (*23*) and *Leishmania donovani* APRT (LdAPRT) (*24*) have been crystallographically determined for the apoenzymes, as well as for the APRT-AMP binary complexes. In the case of the LdAPRT, an APRT−adenine complex was also solved. These structures reveal a number of features common to type I PRTs, including core and hood domanins, as well as a large flexible loop poised to cover the active site. However, the APRT structures reveal a number of structural novelties compared with other purine PRTs, including an unusual purine binding pocket and no apparent candidate for a catalytic base residue located within the active site (*24*). Interestingly, LdAPRT appears to be more structurally related to OPRT than to any of the other purine PRTs. Furthermore, the apparent ability of the *L. donovani* enzyme to form an APRT−adenine binary complex (*23*, *24*) would appear to suggest that the parasite purine salvage enzyme may exhibit a random sequential kinetic mechanism.

To resolve the apparent biochemical and structural dissimilarities between LdAPRT and other purine PRTs and to evaluate the structural model for LdAPRT further, we have analyzed the kinetic mechanism of LdAPRT using kinetic bisubstrate and product inhibition analyses and steady-state fluorescence binding in order to determine the order of substrate binding and product release. Our data suggest that the LdAPRT follows a highly ordered bi−bi kinetic mechanism, where PRPP is the first substrate to bind to the enzyme, followed by adenine. Additionally, we have also established microscopic rate constants for the majority of the individual steps in this mechanism employing pre-steady-state kinetics and transient stopped-flow fluorescence techniques.

EXPERIMENTAL PROCEDURES

Chemicals and Reagents. All chemicals and reagents were purchased from Sigma Chemical Co. unless otherwise noted. DE81 disks (catalog no. 3658323) were bought from Whatman International, Ltd. [^{14}C]Adenine (55 mCi/mmol) was obtained from Moravek Biochemicals, and $^{32}PP_i$ (15 mCi/mmol) was acquired from New England Nuclear Life Sciences Products, Inc. Trinitrophenyl-AMP (TNP-AMP) was purchased from Molecular Probes and spectroscopy-grade HEPES from USB.

Purification of APRT. The *LdAPRT* gene was expressed in *E. coli* strain SΦ446, a clone that lacks the bacterial APRT activity, and recombinant LdAPRT was purified essentially as described (*25*) with the following exception. The purification procedure was augmented with an additional step in which the clarified bacterial 100 000 *g* supernatant in 25 mL of TMD50 (50 mM Tris pH 7.5, 10 mM $MgCl_2$, and 2.5 mM dithiothreitol) buffer was chromatographed over a 40 mL TMD50-equilibrated DEAE-cellulose column, and the column washed continuously with TMD50. Fractions (5 mL) were collected and evaluated for the presence of LdAPRT by sodium dodecyl sulfate−polyacrylamide gel electrophoresis. Fractions containing LdAPRT protein were pooled, chromatographed over a 2.5 mL AMP−agarose column (Sigma catalog no. A-3019), and eluted with TMD50 containing 2 mM PRPP as previously reported for the purification of LdAPRT (*25*). The eluate was then dialyzed for 48 h against two 4 L volumes of TMD50 to remove residual PRPP. Protein concentrations were determined by measuring absorbance at 280 nm ($\epsilon = 16\,960\ M^{-1}\ cm^{-1}$).

Forward and Reverse Assays for LdAPRT Activity. All assays were performed at 27 °C in 100 mM Tris pH 7.5 buffer containing 10 mM $MgCl_2$. In all experiments, LdAPRT measurements were initiated by addition of enzyme. The forward reaction was assayed using both spectrophotometric and radiometric techniques. The spectrophotometric assay was performed with a Beckman DU-640 spectrophotometer, and the absorbance increase associated with the conversion of adenine to AMP was monitored at 256 nm ($\Delta\epsilon = 2.13\ mM^{-1}\ cm^{-1}$) where spectral differences between adenine and AMP are at a maximum. The reaction was performed in a 1 cm quartz cuvette in a final volume of 1.0 mL.

The radiometric assay monitored the conversion of [^{14}C]adenine to [^{14}C]AMP using the filter binding protocol described by Allen et al. (*26*). Buffer and divalent ion conditions were identical to those of the spectrophotometric assay except that the final assay volume was 120 μL. Aliquots (15 μL) of the reaction mixture were spotted at various time points onto DE81 filter disks under constant vacuum suction. Disks were washed thoroughly with H_2O and then 95% EtOH and dried, and radioactive AMP product was quantitated by scintillation spectrometry. Rates for a single LdAPRT reaction were typically determined from seven time points.

AMP pyrophosphorolysis was monitored by coupling PRPP formation to quinolinate phosphoribosylation in the presence of excess *E. coli* quinolate phosphoribosyltransferase (QPRT) using the methodology of Bhatia et al. (*27*). Assays were carried out in 1 mL reaction mixtures and typically contained 0.15 units of recombinant QPRT, 100

μM quinolinate, and varied concentrations of AMP and PP_i. Reactions were terminated at various times by removal of 100 μL of the reaction mixture and rapid mixing with an equal volume of 2 M NaCN. After incubation of the quenched reaction at 25 °C for 10 min, mixtures were assayed spectrophotometrically for the presence of the cyanide adduct of nicotinic acid mononucleotide (*28*).

Cloning, Expression, and Purification of QPRT. The recombinant QPRT employed for the LdAPRT reverse reaction was generated from a *QPRT* construct in the bacterial pBAce expression vector (*29*). PCR was used to amplify *QPRT* from 1 μL of a stationary phase *E. coli* culture using Advantage-HF2 polymerase (Clonetech). The sense primer, 5′-CAT**ATG**CCGCCTCGCCGCTATAAC-3′, harbored an *Nde*I restriction site (underlined), which was inserted at the initiation codon (boldface), while the antisense primer, 5′-TCTAGACTA**TTA**GCGAAAACGCATTG-3′, contained an *Xba*I site (underlined) upstream from the termination codon (boldface). After 30 cycles of denaturation at 94 °C for 30 s, annealing at 68 °C for 1 min, and extension at 68 °C for 8 min, the PCR product was ligated into the PCR2.1-TOPO vector (Invitrogen) and then subcloned into the pBAce vector via *Nde* I and *Xba* I restriction sites. Automated DNA sequencing was performed in both directions to verify the *QPRT* sequence. *QPRT* expression was induced in low phosphate induction (LPI) medium as described (*28*).

JM109 *E. coli* cells transformed with the QPRT expression plasmid were cultured in 1 L of LPI, harvested, and lysed by a French press into 50 mM Tris pH 7.5 buffer with 2mM DTT. The lysate clarified by centrifugation at 100 000 *g* and then chromatographed over a 30 mL DEAE column was equilibrated in the same buffer. Protein was eluted using a 400 mL 0−50 mM $MgCl_2$ gradient. Fractions containing QPRT were pooled and precipitated with 50% $(NH_2)_2SO_4$. The protein was then dialyzed overnight against 4 L of 100 mM Tris pH 7.5 buffer, 10 mM $MgCl_2$, and 100 mM NaCl.

Isotope Exchange Reactions. All isotope exchange half reactions were performed in 100 mM Tris pH 7.5 buffer with 10 mM $MgCl_2$ at 27 °C and were initiated by the addition of 8.5 nmol of LdAPRT. The PRPP−PP_i exchange reaction was performed in a volume of 100 μL and contained 200 μM PRPP and 500 μM $^{32}PP_i$, while the adenine−AMP exchange reaction was carried out in a volume of 1 mL and included 100 μM [^{14}C]adenine and 250 μM AMP. Both exchange reactions were allowed to proceed for 1 h after which 5 μL of the reaction were spotted on 20 cm PEI−cellulose TLC plates (Merck; Darmstadt, Germany) and developed according to the methods of Bhatia et al. (*1*). Radioactivity was measured by phosphorimagery.

Bisubstrate Analysis. Bisubstrate kinetic analyses were performed using the radiometric assay described above for the forward reaction and the QPRT-coupled assay for the backward reaction. Data for initial reaction velocities were fitted to the following equations (*29*) using the KinetAsyst (Intellikinetics) program. For the sequential mechanism:

$$v = V_m[A][B]/(K_{ia}K_{ia}) + K_{ma}[B] + (K_{mb}[A]) + ([A][B]) \quad (1)$$

For the ping-pong mechanism:

$$v = V_m[A][B]/((K_a[B]) + (K_b[A]) + ([A][B])) \quad (2)$$

For the equilibrium-ordered mechanism:

$$v = V_m[A][B]/((K_aK_b) + (K_b[A]) + ([A][B])) \quad (3)$$

The equation that fit the experimental data best was identified by nonlinear least-squares analysis and used for the determinations of steady-state kinetic parameters.

LdAPRT Steady-State Inhibition. The modes of inhibition of AMP and PP_i for the forward reaction and of formycin AMP for the reverse reaction were determined spectrophotometrically. Inhibition patterns were then fitted to one of the following equations by the KinetAsyst program. For competitive inhibition:

$$v = V_m[S]/(K_m(1 + I/K_{is}) + [S]) \quad (4)$$

For noncompetitive inhibition:

$$v = V_m[S]/(K_m(1 + I/K_{is}) + [S](1 + I/K_{ii})) \quad (5)$$

For uncompetitive inhibition:

$$v = V_m[S]/(K_m + [S](1 + I/K_{ii})) \quad (6)$$

Nonlinear least-squares analysis was also used to ascertain which equation best fit the experimental data.

Equilibrium Fluorescence Binding Measurements. All fluorescence measurements were performed in 50 mM HEPES pH 7.5 buffer containing 5 mM $MgCl_2$ at 25 °C. Fluorescence changes accompanying the binding of TNP-AMP to LdAPRT were measured in a 0.5 mL quartz cuvette using a PTI-QM1 model fluorimeter (Photon Technology International). The excitation wavelength was 410 nm (10 nm slit width), and emission was monitored at 546 nm (5 nm slit width). To experimentally determine the K_d of the binding of TNP-AMP to the *L. donovani* APRT, aliquots of an 8.63 mM TNP-AMP stock solution were titrated into a 0.5 mL volume of buffer containing 5 μM LdAPRT protein. Control fluorescence increases after the addition of TNP-AMP to the buffer in the absence of LdAPRT were also measured and these values subtracted from the experimental measurements in the presence of LdAPRT. The data were then fit to the following equation using Kaleidagraph (Apelbeck Software):

$$\%\ \text{fluorescence change} = (F_{max}[\text{TNP-AMP}]/K_d + [\text{TNP-AMP}]) \quad (7)$$

where F_{max} is the maximal fluorescence change, and K_d is the equilibrium dissociation constant for TNP-AMP binding.

Inhibition of fluorescence change was determined by titrating aliquots of AMP, PRPP, or formycin AMP, as appropriate, into 0.5 mL of buffer containing 5 μM TNP-AMP and 1.0 μM LdAPRT. The resulting data were represented as % fluorescence change and fit to the following hyperbolic equation using Kaleidagraph:

$$\%\ \text{fluorescence change} = (F_{max}[\text{ligand}]/K_{d(app)} + [\text{ligand}]) \quad (8)$$

where F_{max} is the maximal fluorescence change and $K_{d(APP)}$ is the apparent equilibrium dissociation constant for competi-

tive ligand binding. Equilibrium constants (K_d) for ligand dissociation were then calculated according to eq 9:

$$K_d = K_{d(APP)}/(1 + [\text{TNP-AMP}]/K_{d(TNP-AMP)}) \quad (9)$$

Pre-Steady-State Kinetics. Pre-steady-state kinetics measurements of the forward reaction were performed on a model SF-61 stopped-flow system (Hi-TECH Scientific) by monitoring the increase in absorbance at 256 nm. All measurements were obtained at 27 °C in 100 mM Tris pH 7.5 buffer containing 10 mM $MgCl_2$ using a two-syringe setup in which LdAPRT preincubated with 250 μM PRPP in one syringe was rapidly mixed with various concentrations of adenine in the other. The absorbance increase at 256 nm as a function of time was described by the following single-exponential equation with a steady-state term:

$$\text{Abs}_{256} = \Delta A e^{-k_{obs}t} + vt \quad (10)$$

where Abs_{256} is the absorbance signal at time t, ΔA is the amplitude in absorbance units of the initial, logarithmic (burst) phase, k_{obs} is the observed first-order rate constant governing the initial burst phase, and v is the rate of increase in absorbance during the second linear (steady state) phase. Data were collected with Kinetasyst 2 and then fit to eq 10 using Kaleidagraph.

Kinetics of Ligand Dissociation. Transient kinetics of ligand dissociation from LdAPRT were measured using stopped-flow fluorescence spectroscopy. These measurements were obtained at 27 °C in 100 mM HEPES pH 7.5 buffer containing 10 mM $MgCl_2$. Typically, one syringe contained LdAPRT preincubated with ligand, while the other syringe contained TNP-AMP. The excitation wavelength was 410 nm, and emitted light was monitored through a 455 nm cutoff filter. Between 12 and 15 traces were obtained for each experiment and averaged, and data were collected with Kinetasyst 2, exported to Kaleidagraph, and fitted to either a single- or double- exponential equation:

$$F_t = \Delta F e^{-k_{obs}t} + F_{eq} \quad (11)$$

$$F_t = \Delta F_1 e^{-k_{1obs}t} + \Delta F_2 e^{-k_{2obs}t} + F_{eq} \quad (12)$$

where F_t is the fluorescence at time t, ΔF_n is the amplitude of fluorescence increase for a given exponential phase, k_{obs} is the observed first-order rate constant for a corresponding phase, and F_{eq} is the fluorescence at equilibrium.

Kinetics of Product Ternary Complex Formation. Steady-state fluorescence measurements were obtained in 50 mM HEPES pH 7.5 buffer containing 5 mM $MgCl_2$ at 25 °C. Fluorescence changes were measured in a 0.5 mL quartz cuvette using a PTI-QM1 model fluorimeter (Photon Technology International). The excitation wavelength was 313 nm (10 nm slit width), and emission was monitored at 360 nm (5 nm slit width). Data were fitted using eq 8 with Kaleidagraph. All stopped-flow experiments were performed at 27 °C on an SF-61 stopped-flow instrument. Typically, one syringe contained LdAPRT preincubated with various concentrations of formycin AMP, while the other contained various PP_i concentrations in buffer. Formycin AMP-associated fluorescence changes due to PP_i binding were monitored through a 320 nm cutoff filter using an excitation wavelength of 313 nm. For each experiment, 12−15 traces were taken, and the data were averaged and then fitted to eq 11 with Kaleidagraph.

RESULTS AND DISCUSSION

Bisubstrate Kinetics. To distinguish whether LdAPRT catalysis occurs through a sequential mechanism involving reversible binding of both substrates prior to catalysis or a ping-pong type mechanism requiring the formation of a covalent enzyme−substrate intermediate, kinetic studies were performed over a range of substrate concentrations. Lineweaver−Burk analysis of rate data for the forward reaction obtained at varied adenine concentrations and various fixed PRPP concentrations displayed convergence of lines above the abscissa consistent with a sequential mechanism that proceeds through the formation of a ternary complex (Figure 1A). A similar pattern was obtained for rate data of the reverse reaction at various AMP concentrations and various fixed PP_i concentration (Figure 1B), again compatible with a sequential mechanism governing LdAPRT catalysis. The steady-state kinetic parameters obtained for both the forward and reverse reactions are summarized in Table 1.

Because the human and *S. cerivisiae* APRTs were previously reported to proceed via a ping-pong mechanism requiring a covalently bound, activated phosphoribosyl intermediate (*18, 21*), the sequential mechanism model for LdAPRT was confirmed by isotope exchange methods. If LdAPRT catalysis were to ensue through a ping-pong mechanism similar to that reported for the human and yeast counterparts, LdAPRT operating in the forward direction should catalyze the reversible dissociation of PP_i from PRPP after the formation of the proposed activated phosphoribosyl intermediate. Correspondingly, the enzyme in the reverse direction should catalyze the abstraction of the adenine ring from AMP after formation of the phosphoribosyl intermediate. However, no evidence for LdAPRT-catalyzed exchange between PRPP and $^{32}PP_i$ was observed, as evinced by the lack of incorporation of $^{32}PP_i$ into the PRPP pool, either in the absence or presence of 100 μM AMP. Likewise, no incorporation of [^{14}C]adenine into AMP was observed when the two compounds were incubated with LdAPRT. However, isotope exchange was observed between the purine base and nucleotide after addition of either 100 μM PP_i or 100 μM PRPP. These results further reinforce the notion that LdAPRT binds both substrates in a reversible, noncovalent fashion prior to catalysis, and, therefore, proceeds through a sequential mechanism.

Steady-State Inhibition. To differentiate among the various types of sequential kinetic mechanisms that could be applicable to LdAPRT, the modes of product inhibition were determined to assess both the order of substrate binding and product release. Inhibition constants for all experiments are presented in Table 1. When AMP inhibition of the forward reaction was evaluated at a fixed saturating adenine concentration, AMP exhibited a competitive inhibition profile versus PRPP substrate ($K_{is} = 39.2 \pm 19.1$ μM) (Figure 2). AMP did not, however, inhibit LdAPRT catalysis at saturating PRPP concentrations, regardless of the adenine concentration (data not shown). These results demonstrate that AMP competes with PRPP for binding to the same form of LdAPRT but binds to a different form of the enzyme than adenine. Within the context of a sequential mechanism, these

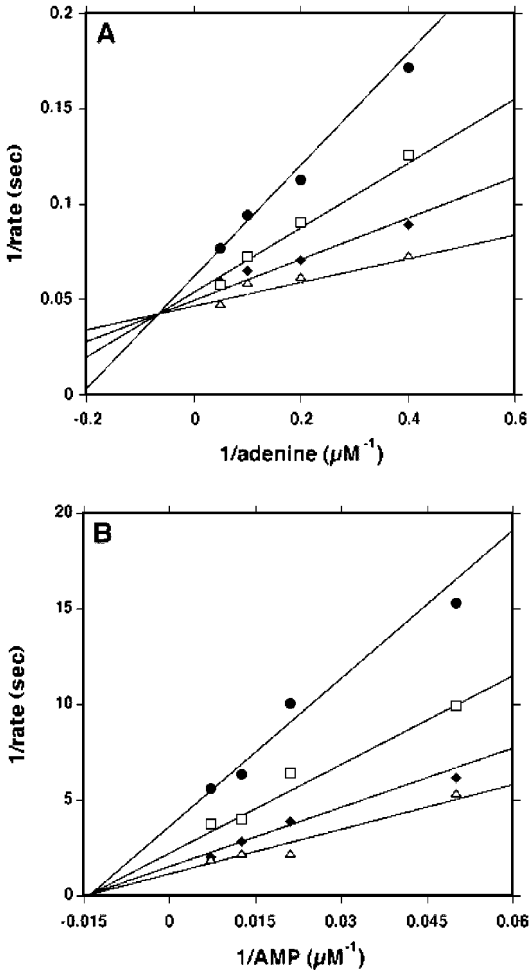

FIGURE 1: Demonstration of ternary complex formation for both forward and reverse LdAPRT reactions. Double-reciprocal plots for the forward (A) and reverse (B) LdAPRT reactions are shown. Experiments for the forward reaction were performed using the radiometric assay described in Materials and Methods. The adenine concentration is varied between 2.5 and 20 μM at various fixed levels of PRPP: 25 μM (closed circles), 50 μM (open squares), 100 μM (closed diamonds), 200 μM (open triangles). Experiments for the reverse reaction were carried out using the QPRT-coupled assay described in Materials and Methods. The AMP concentration is varied between 20 and 140 μM at various fixed levels of PP_i: 75 μM (closed circles), 150 μM (open squares), 300 μM (closed diamonds), 600 μM (open triangles). Both experiments were performed in triplicate with representative plots displayed. Lines were fitted to data from both experiments using KinetAsyst according to the model for a sequential mechanism (eq 1).

Table 1: Steady State Kinetic and Equilibrium Constants for *L. donovani* APRT

substrate	K_d (μM)	K_m (μM)	k_{cat}/K_m (μM^{-1} s^{-1})	k_{cat} (s^{-1})
PRPP	3.83 ± 1.34	25.1 ± 5.9	0.708	
				17.9 ± 5.6 (fwd)
adenine		2.33 ± 1.11	7.66	
PPi		255 ± 168	0.00423	
				1.25 ± 0.82 (rev)
AMP	66.2 ± 15.2	5.23 ± 2.25	0.239	

inhibitor	K_d (μM)	K_{ii} (μM)	K_{is} (μM)
TNP-AMP	1.21 ± 0.22		
formycin AMP	98.7 ± 17.3	89.5 ± 15.8 (vs PP_i)	59.4 ± 22.5 (vs AMP)
			62.3 ± 25.8 (vs PP_i)
AMP (vs PRPP)			39.2 ± 19.1
PP_i (vs PRPP)		242 ± 155	506 ± 120
PP_i (vs adenine)		660 ± 197	526 ± 169

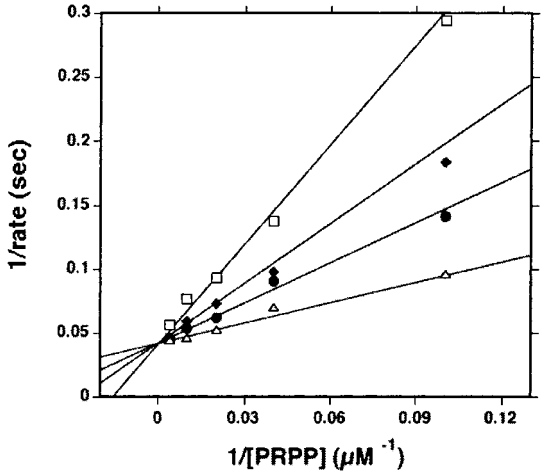

FIGURE 2: AMP is a competitive inhibitor toward PRPP. Experiments were carried out using the spectrophotometric assay described in Materials and Methods. Data are plotted in double-reciprocal form. The adenine concentration is held constant at 50 μM and the PRPP concentration varied between 10 and 200 μM at various fixed levels of AMP: 0 μM (open triangles), 12.5 μM (closed circles), 25 μM (closed diamonds), 50 μM (open squares). The experiment was performed in triplicate with a representative plot displayed. Lines were fitted to the data using KinetAsyst according to the model for competitive inhibition (eq 4).

data are consistent with a model in which PRPP and AMP both bind to the LdAPRT apoenzyme and are, therefore, the first substrate bound and the last product released, respectively. Given this model, the observation that AMP and adenine bind to different LdAPRT forms is explained by a model in which adenine binds only to an LdAPRT−PRPP binary complex.

The steady-state inhibition properties of PP_i versus both PRPP and adenine were also examined. Inhibition profiles at varying PP_i concentrations were observed to be noncompetitive for both PRPP ($K_{ii} = 242 \pm 155$, $K_{is} = 506 \pm 120$) and adenine ($K_{ii} = 690 \pm 197$, $K_{is} = 526 \pm 169$) (Figure 3). This suggests that PP_i binds to a form of LdAPRT distinct from that of PRPP or adenine but that the two forms are coupled in a reversible manner. Together with the AMP inhibition data, these observations argue strongly for a fully ordered reaction mechanism, where initial binding of PRPP to the LdAPRT apoenzyme is followed by adenine binding and catalysis. PP_i is then the first product to be released followed by AMP.

The nature of the QPRT-coupled assay used to measure rates of the pyrophosphorolysis reaction precluded a complete product inhibition analysis for catalysis in the reverse direction. As an alternative, formycin AMP inhibition patterns were, therefore, employed to probe the order of substrate (AMP and PP_i) addition for the reverse reaction. Formycin AMP is a pyrazolopyrimidine analogue of AMP that contains a carbon atom at the 9-position (and a nitrogen at the 8-position), thereby rendering the molecule inert to pyrophosphorolysis. As expected, formycin AMP behaved as a competitive inhibitor against AMP ($K_{is} = 59.4 \pm 22.5$) (data not shown) and as a noncompeitive inhibitor against PP_i ($K_{ii} = 89.5 \pm 15.8$, $K_{is} = 62.3 \pm 25.8$) (Figure 4). These results are consistent with the ordered addition of substrates in the reverse reaction (*30*) and agree with a model

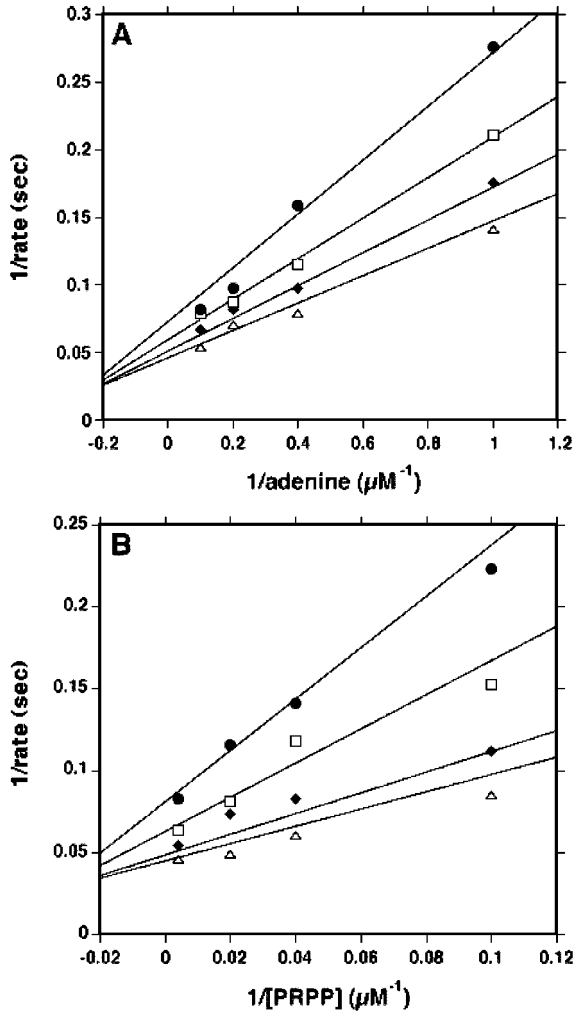

FIGURE 3: Inhibition of LdAPRT by the product PP_i. Data for inhibition of adenine (A) and PRPP (B) are plotted in double-reciprocal form. Both experiments were carried out using the spectrophotometric assay described in Materials and Methods. Experiments for inhibition of adenine were performed with the PRPP concentration held constant at 200 μM and the adenine concentration varied between and μM at various fixed levels of PP_i: 0 M (open triangles), 250 μM (closed diamonds), 500 μM (open squares), 1500 μM (closed circles). Experiments for inhibition of PRPP were performed with the adenine concentration held constant at 60 μM and the adenine concentration varied between 1 and 10 μM at various fixed levels of PP_i: 0 μM (open triangles), 250 μM (closed diamonds), 500 μM (open squares), 1500 μM (closed circles). Both experiments were performed in triplicate, and a representative plot is displayed. In both A and B, lines were fitted to the data using KinetAsyst according to the model for noncompetitive inhibition (eq 5).

in which AMP is not only the final product to leave in the forward reaction but the first substrate to bind in the reverse reaction.

Equilibrium Binding. To determine the affinities of LdAPRT for its substrates and products and to validate the ordered sequential kinetic model suggested by bisubstrate and product inhibition data, equilibrium binding measurements of substrates and products to LdAPRT were carried out. To measure binding affinities of ligands to LdAPRT, a binding assay using TNP-AMP, a fluorescent probe, was implemented. Addition of AMP or PRPP to an LdAPRT/TNP-AMP mixture abrogated the enhanced fluorescence signal elicited by the binding of LdAPRT to the fluorescent

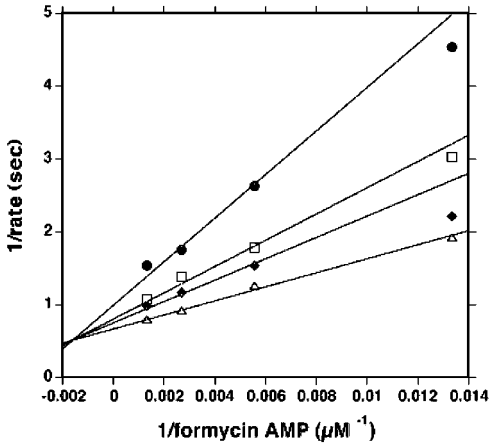

FIGURE 4: Inhibition of the LdAPRT reverse reaction by formycin AMP versus PP_i. Data are plotted in double-reciprocal form. The experiment was carried out using the QPRT-coupled assay described in Materials and Methods. Experiments for inhibition of adenine were performed with the AMP concentration held constant at 100 μM and the PP_i concentration varied between 75 and 750 μM at various fixed levels of formycin AMP: 0 M (open triangles), 50 μM (closed diamonds), 120 μM (open squares), 300 μM (closed circles). The inhibition experiment was performed in triplicate, and a representative plot is displayed. Lines were fitted to the data using KinetAsyst according to the model for noncompetitive inhibition (eq 5).

analogue, demonstrating that TNP-AMP was a useful probe for ascertaining the binding of ligands to the active site of the enzyme. The resulting fluorescence intensity data plotted as a function of TNP-AMP concentration displayed two distinct components: a saturable component resulting from reversible binding of the fluorescent probe to LdAPRT and a linear portion arising from the accumulation of unbound TNP-AMP. Subtraction of the linear component from the biphasic data yielded a saturable hyperbolic curve for the binding of TNP-AMP to LdAPRT (Figure 5A) with a calculated K_d value of 2.21 $\pm$ 0.22 μM.

Affinities of putative ligands of LdAPRT were then determined from their ability to competitively displace TNP-AMP from the enzyme. All competition experiments were conducted with LdAPRT at a 6-fold molar excess with respect to TNP-AMP in order to ensure that all of the TNP-AMP ligand was bound to the enzyme. The percent decrease in fluorescence as a function of PRPP (Figure 5B) or AMP (Figure 5C) concentration revealed K_d values of 3.83 $\pm$ 1.34 μM and 66.2 $\pm$ 15.2 μM for PRPP and AMP, respectively. A K_d value of 98.7 $\pm$ 17.3 μM was calculated for formycin AMP, a value comparable to that obtained for AMP. Conversely, a K_d value of $\sim$1.8 mM was calculated for adenine, while PP_i at concentrations up to 5 mM did not displace TNP-AMP from the enzyme, observations consistent with the ordered sequential binding mechanism model proposed above.

The steady-state kinetic and binding data suggest that PRPP and AMP are the only ligands that bind to the enzyme with affinities capable of supporting catalysis and that an LdAPRT−adenine complex is probably not kinetically viable. While the measurable binding of adenine does imply a random sequential mechanism, the disparity between the measured K_d (1.8 mM) and the K_m measured for adenine (2.33 μM) in steady-state kinetics experiments indicates that the LdAPRT mechanism is effectively ordered and that the

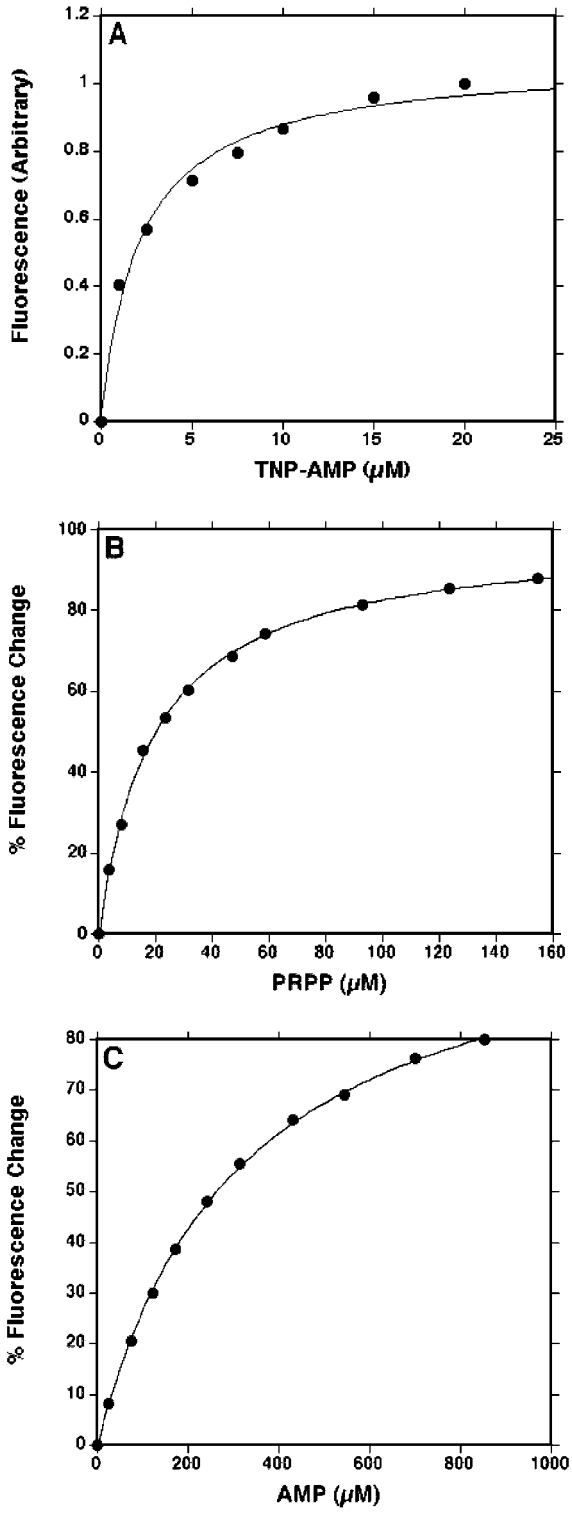

FIGURE 5: Use of TNP-AMP fluorescence to study the equilibrium binding of ligands to APRT. The enhanced extrinsic fluorescence of TNP-AMP upon binding to LdAPRT was observed at 545 nm by excitation at 410 nm. (A) TNP-AMP was added incrementally to a solution containing LdAPRT and fluorescence intensity measured after each addition. Data were treated as described in Materials and Methods and fitted to eq 7 using Kaleidagraph. (B, C) A solution containing 5.0 μM TNP-AMP preincubated with 1.0 μM LdAPRT was titrated with aliquots from concentrated stocks of PRPP (B) and AMP (C). The change in the fluorescence due to competition with ligand was plotted as a % of change in fluorescence from the initial, untitrated solution. Data for both B and C were fitted to eq 8 using Kaleidagraph and used to calculate K_d values as described in Materials and Methods.

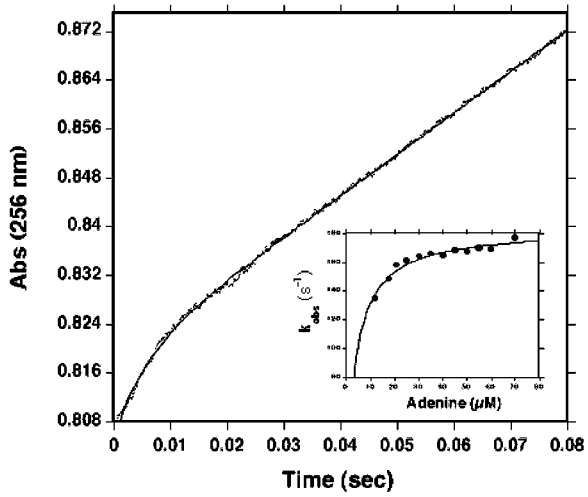

FIGURE 6: Pre-steady-state burst of AMP production as determined by stopped-flow absorbance at 256 nm. Time course of the logarithmic approach to the steady-state rate when a solution containing 11 μM LdAPRT preincubated with 250 μM PRPP was mixed with 70 μM adenine under standard assay conditions. The line represents the fit of the data to eq 10. The inset shows the dependence of k_{obs} upon adenine concentration under fixed LdAPRT and PRPP concentrations. The line represents the fit of the data to eq 13.

kinetic flux through the LdAPRT−adenine binary complex is negligible at concentrations near the adenine K_m. This contrasts with the previous assumption of an ordered mechanism drawn from high-resolution three-dimensional structures of both LdAPRT−adenine and LdAPRT−AMP binary complexes (*24*). However, the content of adenine in the crystallization conditions was at 5 mM, well within range of the adenine affinity observed for the enzyme. An alternative explanation for the crystallographic demonstration of an LdAPRT−adenine binary complex may be that citrate, a component of the crystallization solution that also cocrystallized in the LdAPRT active site with adenine, possibly mimicks PP_i hydrogen bonding, thereby simulating an LdAPRT−PP_i−adenine dead-end ternary complex. In such a complex, the binding affinity for both PP_i and adenine might be greater.

Pre-Steady-State Kinetics. When LdAPRT-dependent AMP formation was monitored at 256 nm by stopped-flow spectrometry, a biphasic time course was observed (Figure 6). The initial "burst" phase was described by a single-exponential term ($k_{obs} = 178 \pm 41$ s^{-1}). The second phase was linear, and a steady-state value of 16.1 ± 3.6 s^{-1} was determined, a value that is in good agreement with the k_{cat} value measured in the steady-state kinetic experiments (Table 1). Both the burst amplitude and linear rates were proportional to the monomeric enzyme concentration, as 2- and 3-fold increases in the enzyme concentration resulted in proportionate increases in both parameters, while the k_{obs} value remained essentially constant in all experiments. The k_{obs} value for the exponential phase displayed a hyperbolic dependence on adenine concentration (Figure 6, inset). The following equation was used to analyze this relationship:

$$k_{obs} = k_{burst}[\text{adenine}]/(K_{app} + [\text{adenine}]) \qquad (13)$$

where maximum k_{obs}, as denoted by k_{burst}, yielded a value of 182 ± 32 s^{-1}. The K_{app} value was calculated to be $5.96 \pm$

1.86 μM and represents the dissociation constant for adenine from the APRT−PRPP−adenine complex. The results from the pre-steady-state experiments are consistent with the notion that phosphoribosyl transfer chemistry is rapid and that some aspect of product release is slower and rate limiting for steady-state turnover. The rapid phosphoribosyl transfer and slow product release is a mechanistic feature common among at least two other type I PRTs, the human HGPRT (*13*) and *S. typhimurium* OPRT (*17*). These data also reinforce the notion of ordered substrate binding, as the binding affinity of adenine for the APRT-PRPP binary complex is dramatically increased over that for the apo-enzyme.

Kinetics of Ligand Dissociation. Dissociation rate constants for LdAPRT−ligand complexes were measured using a competitive displacement technique (*31*). This approach involves mixing preformed enzyme−ligand (E−L1) complex with a large excess of a second ligand (L2) that competes for the same binding site. The rate of any accompanying change in signal as a result of ligand exchange should reflect the dissociation rate of L1 from the enzyme, provided that the association rate of L2 is sufficiently fast. The validity of the measurement as a dissociation rate for L1 can be confirmed by demonstrating that the observed rate is independent of the L2 concentration. Ligand dissociation from LdAPRT was monitored by increases in fluorescence ascribed to the ligand displacement by TNP-AMP on a stopped-flow apparatus. Figure 7A shows an exemplary experimental trace for PRPP dissociation when LdAPRT−PRPP complex was mixed with an excess (>350 μM) of TNP-AMP. The data can be described by a single-exponential term with a k_{obs} value of 3.53 ± 0.98 s^{-1}. Increasing the TNP-AMP concentration 2−3-fold did not affect the observed rate, indicating that the k_{obs} value is independent of TNP-AMP concentration and reflective of the PRPP dissociation rate.

Due to experimental constraints and the relatively low affinity of AMP for LdAPRT (K_d = 66.2 ± 15 μM), experiments measuring the AMP dissociation rate characteristically involved the mixing of TNP-AMP with a solution containing substantial amounts of both unbound and bound APRT. As expected, data traces for AMP dissociation (Figure 7B) displayed two distinct first-order exponential phases. The initial, rapid phase corresponds to the rapid association of TNP-AMP to unbound APRT. The second, slower phase is dependent on AMP dissociation. The ratio of the amplitude of the two phases (0.57) was close to the calculated ratio of bound to unbound enzyme (0.37), and the amplitude of both phases increased, as expected, when more LdAPRT was added. Adjustment of the TNP-AMP concentration had no significant effect on the second phase, which was assigned a k value of 21.6 ± 4.5 s^{-1} after fitting the data to eq 13.

Despite the relatively low binding affinity of LdAPRT for AMP, the measured rate of AMP dissociation is relatively slow (21.6 s^{-1}) and probably represents the rate-limiting step in the steady-state turnover, given its concordance with the k_{cat} value of 17.8 s^{-1} measured in steady-state experiments. Slow release of nucleotide is also a feature common to several other type I PRT enzymes (*13, 17*). In a detailed kinetic analysis, the pre-steady-state burst observed with the human HGPRT was attributed to the slow, rate-limiting

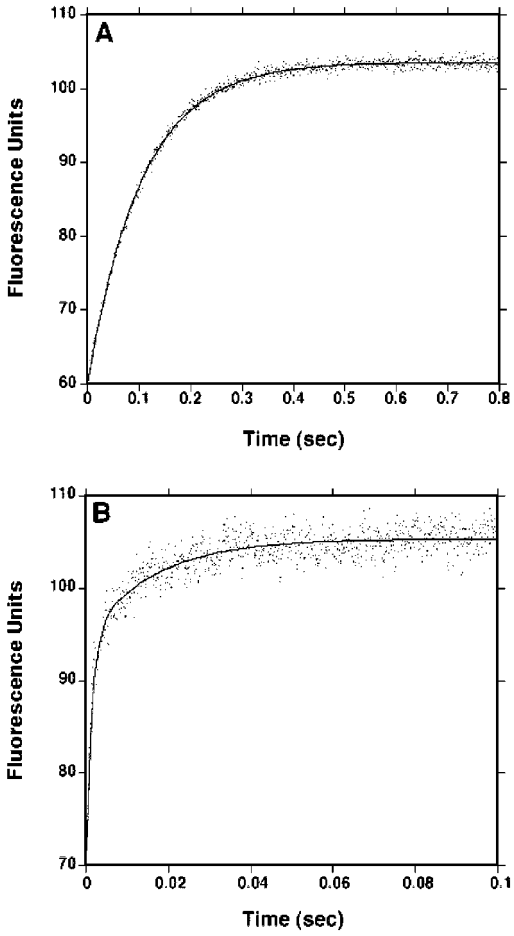

FIGURE 7: Kinetics of PRPP dissociation. Time-course of fluorescence increase when LdAPRT−ligand complex is mixed rapidly with excess TNP-AMP to form LdAPRT−TNP-AMP. (A) PRPP off-rate determination. Final, post-mixing concentrations are 12.8 μM APRT, 55 μM PRPP, 385 μM TNP-AMP. (B) AMP off-rate determination. Post-mixing concentrations are 12.8 μM LdAPRT, 170 μM AMP, 385 μM TNP-AMP. For both experiments, TNP-AMP was excited at 410 nm and emission was monitored using a 455 nm cutoff filter. Data are the average of 12 separate trials. The line represents the fit of the data to eq 11 (for PRPP experiments) and eq 12 (for AMP experiments) using Kaleidagraph.

dissociation of nucleotide from the enzyme (*13*). The pre-steady-state burst kinetics presented here also support the conjecture that LdAPRT proceeds via a similar mechanism and agree with the results of the bisubstrate and fluorescence binding experiments that predict AMP release as the final step in the LdAPRT reaction mechansim.

Kinetics of Product Ternary Complex Formation. Due to its high intrinsic fluorescence, formycin AMP serves as a useful probe for studying the behavior of AMP binding proteins (*32*). However, no significant change in formycin AMP emission was observed when the pyrazolopyrimidine analogue was mixed with LdAPRT at excitation wavelengths between 290 and 315 nm, wavelengths which yielded the greatest emission at >320 nm. Interestingly, when the preformed LdAPRT−formycin AMP complex (12 μM APRT and 215 μM formycin AMP) was mixed with PP_i, a distinct decrease in fluorescence emission was observed when the sample was excited at 313 nm. This PP_i-induced quenching of formycin AMP fluorescence was detected only in the presence of LdAPRT. The change in formycin AMP

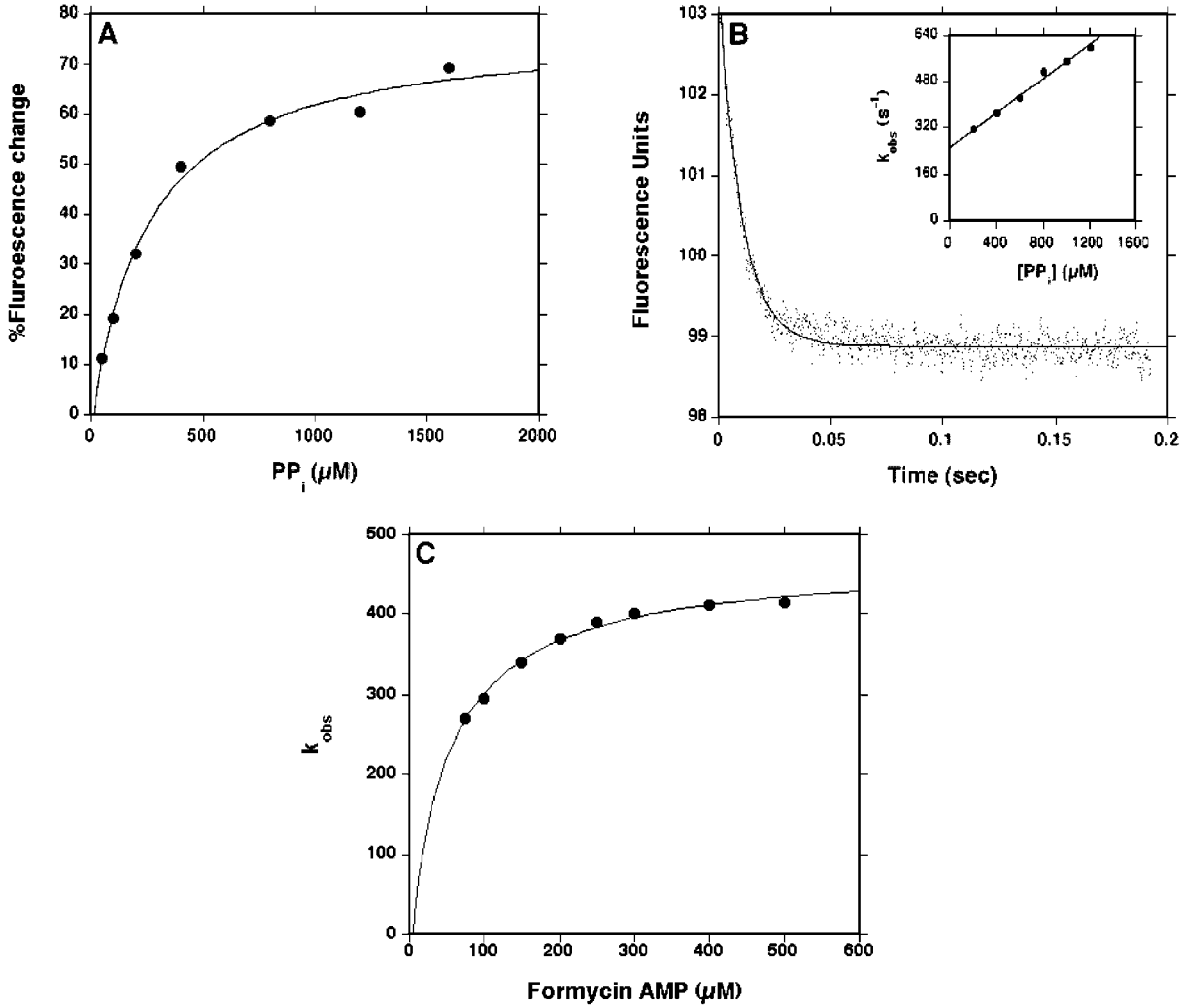

FIGURE 8: Kinetics of Formycin AMP−PP_i−LdAPRT complex formation. (A) The enhanced extrinsic fluorescence of formycin AMP−LdAPRT upon binding to PP_i was observed at 365 nm by excitation at 313 nm. PP_i was added incrementally to a solution containing LdAPRT (12 μM) and formycin AMP (215 μM) and fluorescence intensity measured after each addition. The decrease in the fluorescence due to quenching of formycin AMP fluorescence was plotted as a % of decrease in fluorescence from the initial, untitrated solution. Data were fitted to eq 8 using Kaleidagraph to yield a hyperboloidal plot. (B) Time-course of fluorescence increase when solution containing LdAPRT−formycin AMP is mixed rapidly with a solution containing PP_i to give LdAPRT−formycinAMP−PP_i. Post-mixing concentrations for a typical experiment were 15 μM LdAPRT and 250 μM formycin AMP. Formycin AMP was excited at 313 nm, and fluorescence was read through a 320 nm cutoff filter. The trace in the figure is a representative experiment conducted at a concentration of 200 μM PP_i and is the average of 13 trials. The line represents the fit of the data to eq 11 using Kaleidagraph. The inset shows values for k_{obs} for various PP_i concentrations fitted to a linear model according to eq 14. (C) Relationship between k_{obs} and formycin AMP concentration for similar stopped-flow experiments. For each experiment, LdAPRT and PP_i concentrations were held constant at 25 and 850 μM, respectively. Kaleidagraph was used to generate the hyperboloidal plot that was fitted to the data with eq 15.

fluorescence as a function of PP_i concentration is depicted in Figure 8A. This hyperbolic relationship was then fitted to eq 8, and a K_{app} value for PP_i-induced quenching of 282 ± 56 μM was calculated. The PP_i-induced quenching of formycin AMP fluorescence as a function of time is shown in Figure 8B. This trace fits well with the first-order exponential described by eq 11. The calculated value for k_{obs} shows a linear dependence on PP_i concentration (Figure 8B inset). The following equation was used to obtain rate values for the quenching event (*5*):

$$k_{obs} = k_i[PP_i] + k_{-1} \quad (14)$$

where k_1 and k_{-1} are the rate constants governing PP_i association and dissociation, respectively. Rate constants of 0.349 ± 0.067 μM^{-1} s^{-1} and 255 ± 38 s^{-1} were calculated for PP_i association and dissociation, respectively, yielding a k_{-1}/k_1 value of 730 μM. These data support the conclusion that the quenching event was reflective of PP_i association with the LdAPRT−formycin AMP complex. The low apparent affinity of PP_i for the LdAPRT−formycin AMP binary complex and the fast dissociation rate of PP_i are consistent with the high K_i values observed in the steady-state inhibition experiments and provide further evidence that PP_i dissociation is the preferential first step in product release. Interestingly, the nearly 3-fold discrepancy between the k_{-1}/k_1 ratio and the thermodynamic equilibrium constant (K_{app} = 282 ± 56 μM) intimates that there is another step to binding that is not monitored by this experiment. However, the nonsaturability of the plot for k_{obs} versus PP_i (inset of Figure 8B) at concentrations >1 mM indicates that the observed change in formycin AMP fluorescence appropriately reflects the PP_i binding event despite any isomerizations that may occur following initial PP_i binding.

Scheme 1: Proposed Kinetic Mechanism for Adenine Phosphoribosyltransferase from *L. donovani*

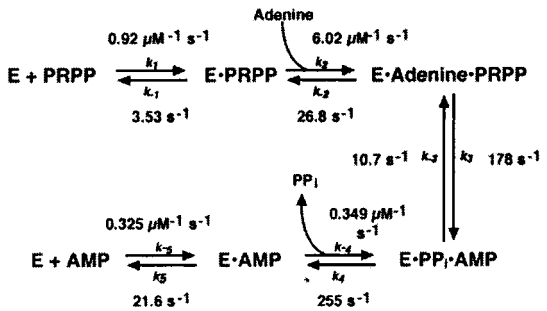

In a separate set of experiments, formycin AMP fluorescence quenching was monitored when a solution of LdAPRT (25 μM) was mixed with a solution of PP_i (850 μM) containing 75−500 μM formycin AMP. The time-dependent formycin AMP quenching is described by a single-exponential term that varied with formycin AMP concentration. When k_{obs} was plotted as a function of formycin AMP concentration, a hyperboloidal (Figure 8C) relationship was observed that could be described by the equation below:

$$k_{obs} = k_{max}[\text{formycin AMP}]/(K_{app} + [\text{formycin AMP}]) \quad (15)$$

The K_{app} value measured for this equilibrium (59.4 ± 12.5 μM) was interpreted as a measure of the equilibrium of formycin AMP dissocation from the enzyme and was close to the K_d value of 98.7 ± 17.3 μM obtained from the steady-state binding measurements. This result reinforces the idea that PP_i binds to a preformed APRT−formycin AMP complex to induce the fluorescence changes.

Calculation of Rate Constants and Kinetic Simulation. On the basis of the data accumulated in this study, the ordered bi−bi kinetic mechanism summarized in Scheme 1 was proposed and the rate constants for each of the individual steps were either measured or calculated. Time-resolved ligand competition experiments demonstrated a rate of PRPP dissociation (k_{-1}) from LdAPRT of 3.53 s^{-1} (see Scheme 1). From this dissociation rate and the K_d of PRPP (3.83 μM) for the enzyme, a value of 0.92 μM^{-1} s^{-1} was obtained for the PRPP association constant (k_1). As predicted for an ordered bi−bi mechanism, k_1 is in good agreement with the k_{cat}/K_m ratio (0.708 μM^{-1} s^{-1}) measured for PRPP in steady-state experiments. A value of 21.6 s^{-1} was obtained for the rate of AMP dissociation (k_5) from the enzyme. A rate of AMP association (k_5) to LdAPRT of 0.325 μM^{-1} s^{-1} was then calculated from the K_d for AMP dissociation (66.2 μM), a value comparable to the k_{cat}/K_m ratio of 0.239 μM^{-1} s^{-1} calculated for AMP in the reverse reaction. Rate constants for PP_i dissociation (k_4 = 255 s^{-1}) and association (k_{-4} = 0.349 μM^{-1} s^{-1}) were then estimated from the stopped-flow experiments measuring association of PP_i to the LdAPRT−formycin AMP complex (see eq 15). The rate of phosphoribosyltransfer chemistry (k_3) of 178 s^{-1} was obtained directly from the pre-steady-state stopped-flow experiments, while the dependence of the burst magnitude on the adenine concentration permitted the measurement of the equilibrium dissociation constant (k_{-2}/k_2) for adenine binding to the LdAPRT−PRPP complex of 5.98 μM. The following equations for a bi−bi mechanism with ordered substrate addition

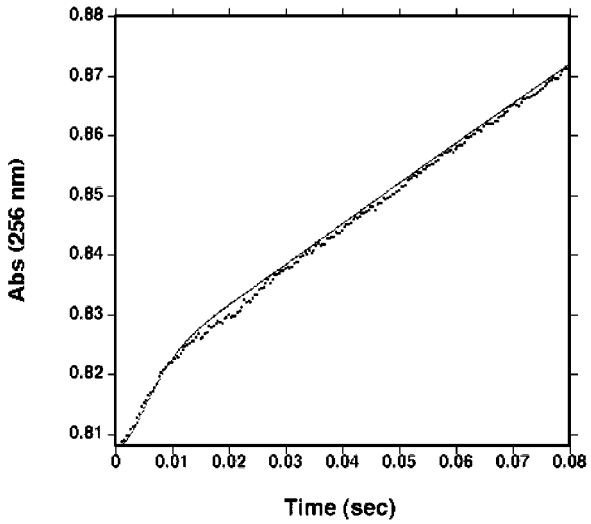

FIGURE 9: Simulation of the time course for the LdAPRT reaction as measured by stopped-flow absorbance. The data trace shows the approach to the steady-state rate obtained when when 11 μM APRT preincubated with 250 μM PRPP was mixed with 70 μM adenine. The solid line was simulated with KINSIM using the kinetic model and rate constants depicted in Scheme 2. Output for the simulation was calculated for the accumulation of the LdAPRT−AMP−PP_i, LdAPRT−AMP, and AMP species.

and product release and central complex isomerization were then used to calculate k_{-2} and k_{-3} (*33*):

$$k_{-2} = k_{-1}k_{cat(rev)}(k_3 + k_{-3})/k_{-1}k_{-3} - k_{cat(rev)}(k_{-1} + k_{-3}) \quad (16)$$

$$k_{-3} = (k_4k_5k_3) - k_{cat(fwd)}(k_4k_5 + k_4k_3 + k_5k_3)/k_{cat(fwd)}k_4 \quad (17)$$

The calculated values for k_{-2} and k_{-3} were 26.8 s^{-1} and 10.7 s^{-1}, respectively. The rate of adenine association to the LdAPRT−PRPP binary complex (k_2) of 6.02 μM^{-1} s^{-1} was then obtained from the k_{-2} *v*alue and the k_{-2}/k_2 ratio.

As microscopic rate constants for all the steps depicted in Scheme 1 were either directly measured or reasonably deduced, it is possible to use these constants to calculate K_m values for all substrates of both the forward and reverse reactions. Employing the equations derived by Plapp (*33*) gave K_m values of 17.8 and 3.58 μM for PRPP and adenine, respectively, numbers similar to the experimentally determined K_m values of 25.1 ± 5.9 and 2.33 ± 1.11 μM obtained from the steady-state analyses. For the reverse reaction, K_m values for PP_i and AMP were calculated to be 473 and 2.95 μM, respectively, numbers comparable to the 295 ± 168 and 5.23 ± 2.25 μM experimentally obtained values. Thus, the concordance of the calculated and experimentally obtained K_m values for all substrates validates the proposed bi−bi ordered kinetic mechanism.

To further substantiate the proposed kinetic model for LdAPRT, the pre-steady-state burst kinetics of the enzyme were compared to a computer-simulated time course of the enzyme predicted from the mechanism and rate constants depicted in Scheme 1. Figure 9 shows the stopped-flow absorbance data from the pre-steady-state experiment depicted in Figure 6. The solid line in Figure 9 represents simulated data generated by KINSIM(34) using the mechanism and rate constants shown in Scheme 1. The simulated data represents the predicted accumulation of LdAPRT−

AMP−PP_i, LdAPRT−AMP, and AMP species given the initial concentrations of substrate and enzyme employed in the original experiment. The rate constants in Scheme 1 accurately predict the burst phase of the time course, while the slope of the linear phase of the experimental data differs only slightly from that of the simulation (Figure 9).

Comparison of the LdAPRT Kinetic Mechanism with the LdAPRT Three-Dimensional Structures: The crystallographically determined three-dimensional structures of LdAPRT can now be evaluated within the context of the proposed kinetic model. On the basis of the LdAPRT−adenine binary crystallographic complex, it was initially proposed that the apparent accessibility of both adenine and PRPP binding sites to solution was indicative of a random addition mechanism (*24*). However, the data reported herein demonstrate that substrate binding is highly ordered. The dramatic increase in the affinity of LdAPRT for adenine upon PRPP binding would suggest that the adenine binding pocket, reconfigured upon the binding of PRPP, may be significantly different structurally from that of either the AMP− or adenine−LdAPRT binary complexes. The structural basis for such a mechanism has also been described previously for other type I PRT enzymes (*3*, *35*) and is particularly well illustrated by the *Toxoplasma gondii* HGXPRT, where PRPP binding induces the structural reordering of two active site loops resulting in the formation of the binding pocket, which subsequently accommodates the purine base (*35*). Three-dimensional structures of both substrate and product ternary complexes will further elucidate the conformational changes that LdAPRT undergoes during catalysis and the mechanism through which these changes facilitate adenine binding.

As predicted from the LdAPRT structures, additional isomerizations of the central complex (the conversion of bound substrates to products) depicted in Scheme 1, involving the closure of the large flexible loop over the active site, probably occur prior to and after phosphoribosyltransfer (*24*). While the loop is open and largely disordered in the crystal structures, it almost certainly moves to cover the active site during catalysis, as supported by the presence of several highly conserved amino acid residues in the loop among APRTs from a variety of phylogenetically diverse organisms (*24*). These residues are thought to play critical roles in catalysis, as point mutations at the conserved sites in the mouse (*36*) and *S. cerevisiae* (*37*) APRTs significantly increase the K_m value for adenine and decrease the overall turnover rate of the enzyme. However, since these data provide no convincing evidence for any additional isomerizations of the species depicted in Scheme 1, the relative kinetic lifetimes of either "closed-" or "open-loop" APRT conformations remain unclear. For *S. typhimurium* OPRT, a combination of pre-steady-state quench-flow kinetics and NMR titration techniques have been used to measure the isomerization rate of the flexible loop upon PRPP binding (*38*). Data from these experiments indicate that the loop exists in two discrete (open and closed) conformations when PRPP is bound to the enzyme and that isomerization between OPRT forms is extremely rapid (k_{close} = 12 000 s^{-1} and k_{open} = 400 s^{-1}). The rapidity of these events would probably render any isomerization associated with the movement of the LdAPRT flexible loop undetectable using the experimental approaches employed in this study. Indeed, the rate of central complex isomerization measured in pre-steady-state experiments may reflect the slowest of several distinct kinetic steps that follow adenine association. Determining the three-dimensional structure of a closed-loop transition state LdAPRT complex, as has been accomplished for several other purine PRTs (*39*−*41*), would provide critical insight into the influence of PRPP and adenine binding to the movement of the LdAPRT flexible loop.

REFERENCES

1. Weber, G., Jayaram, H. M., Pillwein, K., Nasumeda, Y., Reardon, M. A., and Zhen, W. S. (1987) *Adv. Enzyme Regul. 26*, 335−52.
2. Berens, R. L., Drug, E. C., and Marr, J. J. (1995) In *Biochemistry and Molecular Biology of Parasites* (Marr, J. J., Müller, M., Eds.) pp 89−117, Academic Press Ltd., London, U.K.
3. Craig, S. P., III, and Eakin, A. E. (2000) *J. Biol. Chem. 257*, 20231−20234.
4. Eads, J. C., Scapin, G., Xu, Y., Grubmeyer, C., and Sacchettini, J. C. (1994) *Cell 78*, 325−324.
5. Scapin, G., Ozturk, D. H., Grubmeyer, C., and Sacchettini, J. C. (1995) *Biochemistry 34*, 10744−10754.
6. Heroux, A., White, L., Ross, L. J., Davis, R. L., and Borhani, D. W., (1999) *Biochemistry 38*, 14495−14506.
7. Schumacher, M. A., Carter, D., Scott, D. M., Roos, D. S., Ullman, B., and Brennan, R. G. (1998) *EMBO J. 17*, 3219−3232.
8. Natalini, P., Santarelli, I., Rugguierri, S., Vita, A., and Magni, G. (1979) *J. Biol. Chem. 254*, 1558−1563.
9. Ali, L. Z., and Sloan, D. L. (1982) *J. Biol. Chem. 257*, 1149−1155.
10. Krentisky, T. A., and Papaioannou, R. (1969) *J. Biol. Chem. 244*, 1271−1277.
11. Henderson, J. F., Brox, L. W., Kelly, W. N., Rosenbloom, F. M., and Seegmiller, J. E. (1968) *J. Biol. Chem. 243*, 2514−2522.
12. Giacomello, A., and Salerno, C. (1978) *J. Biol. Chem. 253*, 6038−6044.
13. Xu, Y., Eads, J., Sacchettini, J. C., and Grubmeyer, C. (1997) *Biochemsitry 36*, 3700−3712.
14. Yuan, L., Craig, S. P., III, McKerrow, J. H., and Wang, C. C. (1992) *Biochemistry 36*, 3700−3712.
15. Mungala, N. R., Chin, M. S., and Wang, C. C. (1998) *Biochemistry 37*, 4045−4051.
16. Bhatia, M. B., Vinitsky, A., and Grubmeyer, C. (1990) *Biochemistry 29*, 10480−10487.
17. Wang, G. P., Lundegaard, C., Jensen, K. F., and Grubmeyer, C. (1999) *Biochemistry 38*, 275−283.
18. Groth, D. P., and Young, L. G. (1971) *Biochem. Biophys. Res. Commun 43*, 82−87.
19. Kenimer, J. G., Young, L. G., and Groth, D. P. (1975) *Biochim. Biophys. Acta 384*, 87−101.
20. Queen, S. A., Vander Jagt, D. L., and Reyes, P. (1989) *Biochim. Biophys. Acta 996*, 160−165.
21. Alfonzo, J. D., Sahota, A., and Taylor, M. W. (1997) *Biochim. Biophys. Acta 1341*, 173−182.
22. Thomas, C. B., Arnold, W. J., and Kelley, W. N. (1973) *J. Biol. Chem. 241*, 1406−1411.
23. Shi, W., Tanaka, K. S. E., Crother, T. R., Taylor, M. W., Almo, S. C., and Schramm, V. L. (2001) *Biochemistry 40*, 10800−10809.
24. Phillips, C. L., Ullman, B., Brennan, R. G., and Hill, C. P. (1999) *EMBO J. 18*, 3533−3545.
25. Allen, T., Hwang, H. Y., Wilson, K., Hanson, S., Jardim, A., and Ullman, B. (1995) *Mol. Biochem. Parasitol. 74*, 99−103.
26. Allen, T., Henschel, E. V., Coons, T., Cross, L., Conley, J., and Ullman, B. (1989) *Mol. Biochem. Parasitol. 33*, 273−81.
27. Bhatia, R., and Calvo, K. C., (1996) *Arch. Biochem. Biophys. 325*, 270−278.
28. Craig, S. P., Yean, L., Kuntz, D. A., McKerrow, J. H., and Wang, C. C. (1991) *PNAS* 88, 2500−2504.

29. Cleland, W. W. (1977) *Adv. Enymol. Relat. Areas Mol. Biol. 45*, 273−387.
30. Fromm, H. J. (1979) *Methods Enzymol. 63*, 467−486.
31. Dunn, S. M. J., Batchelor, J. G., and King, R. W. (1978) *Biochemistry 17*, 2356−2364.
32. Kierdaszuk, B., Modrak-Wojcik, A., Wierzchowski, J., Sugar, D. (2000) *Biochim. Biophys. Acta 1476*, 109−128.
33. Plapp, B. V. (1973) *Arch. Biochem. Biophys. 156*, 112−114.
34. Barshop, B. A., Wrenn, R. F., and Frieden, C. (1983) *Anal. Biochem. 130*, 134−145.
35. Héroux, A., While, L., Ross, L. J., Davis, R. L., and Borhani, D. W. (1999) *Biochemistry 38*, 14485−14494.
36. Khattar, N. H., Jennings, C. D., Walker, K. A., and Turker, S. T. (1995) In *Purine and Pyrimidine Metabolism in Man VIII* (Sahota, A., and Taylor, M. W. Eds.) pp 665−670, Plenum Press, New York.
37. Crother, T. R., and Taylor, M. W. (1998) In *Purine and Pyrimidine Metabolism in Man IX* (Griesmacher, A., Chiba, P., and Müller, M. M., Eds.) pp 229−303, Plenum Press, New York.
38. Wang, G. P., Cahill, S. M., Liu, X., Girvin, M. E., and Grubmeyer, C. (1999) *Biochemistry 38*, 284−296.
39. Focia, P. J., Craig, S. P., and Easkin, A. E. (1998) *Biochemistry 37*, 17120−17127.
40. Balendiran, G. K., Molina, J. A., Xu, Y., Torres-Martinez, J., Stevens, R., Focia, P. J., Eakin, A. E., Sacchettini, J. C., and Craig, S. P. (1999) *Protein Sci. 8*, 1023−1031.
41. Héroux, A., White, L. E., Ross, L. J., Kuzin, A. P., and Borhani, D. W. (2000) *Structure 8*, 1309−1318.

BI0158730